Aerosol Deposition of Thin-Film Single- and Bi-layered Solid Electrolytes for Intermediate Temperature Planar Solid Oxide Fuel Cells

ECS Transactions, 103 (1) 1695-1703 (2021)
10.1149/10301.1695ecst ©The Electrochemical Society

Aerosol Deposition of Thin-film Single- and Bi-layered Solid Electrolytes for Intermediate Temperature Planar Solid Oxide Fuel Cells

I. S. Erilin[a], I. N. Burmistrov[a,b], D. A. Agarkov[a,b], V. E. Pukha[c], D. V. Yalovenko[a], N. V. Lyskov[c], M. N. Levin[d], and S. I. Bredikhin[a,b]

[a] Institute of Solid State Physics RAS, Chernogolovka, Moscow District 142432, Russia
[b] Moscow Institute of Physics and Technology, Dolgoprudniy, Moscow District 141701, Russia
[c] Institute of Problems of Chemical Physics RAS, Chernogolovka, Moscow District 142432, Russia
[d] EFKO Group, Biruch Innovation Center, Malobykovo, Belgorod District 309927, Russia

The aerosol deposition (AD) method is a technique for the formation of thin or thick, gas-tight or porous layers by deposition of microscopic powder particles. In the present work, AD was used to deposit thin-film electrolyte and protective buffer layers for planar anode-supported solid oxide fuel cells (SOFCs). The high quality of the deposited layers was confirmed by scanning electron microscopy, as well as electrochemical measurements, including measurements of current-voltage characteristics and impedance spectroscopy. At a working temperature of 800 °C, the anode-supported cell with a bi-layered electrolyte deposited by AD demonstrated an open-circuit voltage of more than 1.04 V, as well as specific power of more than 780 mW/cm^2. The difficulties, advantages, and peculiarities associated with the formation of thin-film electrolyte and buffer layers of SOFCs by the AD method have been discussed.

Introduction

One of the main limiting factors with regards to increasing in the specific power and efficiency of solid oxide fuel cells (SOFCs) is the development of deposition techniques for the application of thin-film gas-tight electrolytes (1). Hence, the development of inexpensive, repeatable, and scalable technologies to form thin-film electrolytes is a key direction for SOFC improvement. Despite the existence of well-developed industrial techniques, such as chemical vapor/solution deposition (CVD/CSD) (2), electrochemical deposition (ED) (3), thermal spray (TS) (4), and physical vapor deposition (PVD) (5), all of them require high deposition temperatures or high vacuum, which equates to an increase in the cost of deposition setup and the process itself. Aerosol deposition (AD), also known as vacuum kinetic spraying (VKS), is a technique for deposition of thin or thick, gas-tight or porous layers (6). Deposition occurs due to the impact of high-energy particles onto a substrate and their consequent fragmentation and consolidation. This phenomenon is called room temperature impact consolidation (RTIC) (7). The AD method is distinguished by the ability to form thin or thick, gas-tight or porous nanocomposite ceramic films by using

a high-energy aerosol jet at low vacuum (1 – 1000 Pa) and room temperature. In addition, the AD method is characterized by low equipment costs and easy scaling.

The post-treatment temperatures of electrolyte films can be significantly reduced when deposited by AD in comparison with such techniques of film formation as screen-printing, ink-jet printing, and other wet-ceramic methods. For example, J. Exner et al. demonstrated that in the case of an 8 mol.% yttria-stabilized zirconia (8YSZ) electrolyte deposited by AD, good conducting properties of the membrane can be reached at sintering temperatures as low as 900 °C (8, 9). Our team obtained a gas-tight 8YSZ thin-electrolyte layer deposited by AD at sintering temperatures of 1100 – 1200 °C (10), whereas membranes formed by screen-printing or ink-jet printing required sintering temperatures in the range of 1300 – 1400 °C (11, 12), and even films deposited by magnetron sputtering could not be effectively used without some heat treatment (13). The ability to deposit gas-tight films and films with controlled porosity without any additives in a wide range of thicknesses makes it possible to create all of the functional SOFC layers without intermediate sintering steps and even achieve one-step *in-situ* sintering of the entire cell. In addition, lowering electrolyte sintering temperatures will have a positive effect on the geometry of sintered SOFCs, as high-temperature exposure of anode-supported SOFCs, as well as electrolyte deposition by some sputtering methods, leads to deformation of larger cells and further problems with their assembly into stacks (14). The main drawback of the AD method is the strong dependence on powder and substrate hardness and morphology, as well as on the geometry of the AD apparatus, which makes it difficult to replicate the process when parameters change slightly. In the present work, the aerosol deposition technique was used to deposit thin-film electrolyte and protective buffer layers for anode-supported SOFCs.

Experimental

General Information about Manufacturing of the SOFCs

Two types of anode-supported SOFCs were manufactured. Both types of cells were button cells with a diameter of 21 mm.

Type-1. A thin-film 8YSZ electrolyte (SOFCMAN, China), deposited on a bi-layered anode substrate NiO/8YSZ: current-collecting and functional sublayers with a thickness of 450 μm (KCeraCell CO., Korea) using the AD method followed by screen-printing of a composite cathode with the composition of $(La_{0.8}Sr_{0.2})_{0.95}MnO_{3-\delta}$ (LSM) synthesized using the glycine-nitrate technique and zirconia co-stabilized with 10 mol.% scandia and 1 mol.% yttria (10Sc1YSZ) (DKKK Co., Japan). The cathode was sintered in air at 1100 °C. The sintering temperature for the 8YSZ layer was 1300 °C.

Type-2. A bi-layered thin electrolyte made of 8YSZ (SOFCMAN, China) and 10 mol.% gadolinia doped ceria (GDC) (FuelCellMaterials Co., USA) protective layer deposited on the bi-layered anode substrate (KCeraCell Co., Korea) using the AD method, followed by screen printing of an active cathode with the composition of $(La_{0.80}Sr_{0.20})_{0.95}CoO_{3-\delta}$ (LSC) (KCeraCell Co., Korea). The cathode was sintered *in-situ* during initial testing of the cell at 950 °C. The sintering temperatures for the 8YSZ and GDC layers were 1300 °C and 1200 °C, respectively.

The cells were investigated by scanning electron microscopy (Supra 50VP, Zeiss, Germany) as well as by electrochemical measurements including current-voltage characteristics and impedance spectroscopy performed using an Autolab PGSTAT302N instrument equipped with a FRA32 module (Metrohm, Switzerland). The impedance spectra were collected in a frequency range from 0.1 Hz up to 300 kHz at 20 mV voltage amplitude.

The AD Parameters Specification

The deposition process consisted of two main stages: powder preparation (15) and aerosol deposition of the films. Powder preparation included the following steps: annealing, milling, drying, and grinding. SEM images of the resulting powder are shown in Figure 1. The powders consist of small crystallites with a size of less than 100 nm aggregated into relatively hard particles with a size of up to several micrometers. The powder was dispersed through a mesh directly before deposition to break up soft agglomerates.

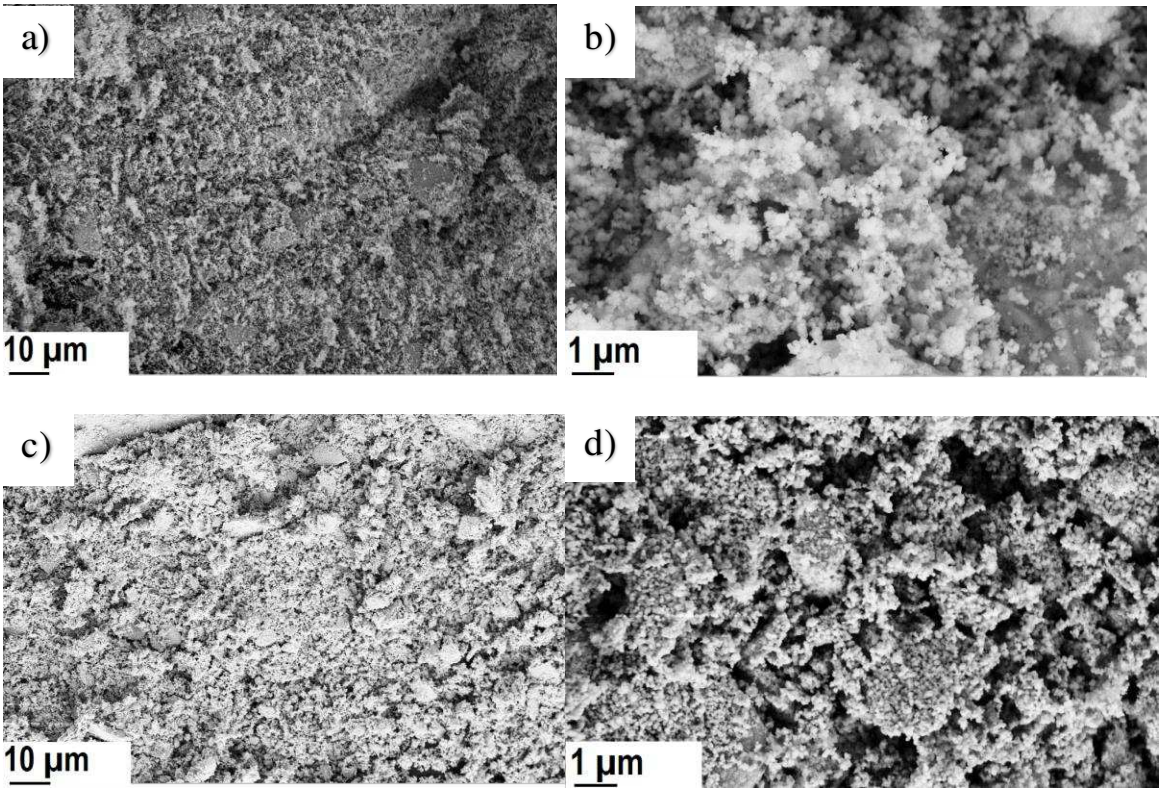

Figure 1. (a), (b) 8YSZ (SOFCMAN) powder after preparation, (c), (d) GDC (FCM) powder after preparation.

A schematic of the AD equipment is shown in Figure 2. During the deposition process, the carrier gas flowed into the aerosol chamber where the powder to be deposited was placed. The deposition chamber rested on a vibrating table for active aerosol generation. The aerosol flowed into the nozzle where it was accelerated to near sound velocities and ejected into the deposition chamber towards the substrate. The nozzle could be directed toward the substrate at different angles to clean deposited agglomerates from the surface during film formation and to avoid defects. When the accelerated particles hit the substrate,

they commonly undergo fragmentation, mechanical adhesion, and subsequent consolidation due to the impact of the subsequent particles. Moreover, J. Akedo proposed that crystallites may be subjected to parameters that favor brittle-ductile transition and force particles to undergo plastic deformation (16). The parameters of AD used during the deposition of the bi-layered electrolyte are shown in TABLE I.

TABLE I. Parameters of AD Used in the Current Research.

Parameter	Value
Pressure in Deposition Chamber	400 Pa
Pressure in Front of the Nozzle	2.5 bar
Nozzle Throat Diameter	1 mm
Nozzle Exit Diameter	3 mm
Angle Between Nozzle and Substrate (90° – Perpendicular Direction of the Nozzle to the Substrate)	40° (8YSZ), 60° (GDC)
Distance Between Nozzle and Substrate	10 mm
Gas-carrier	Nitrogen

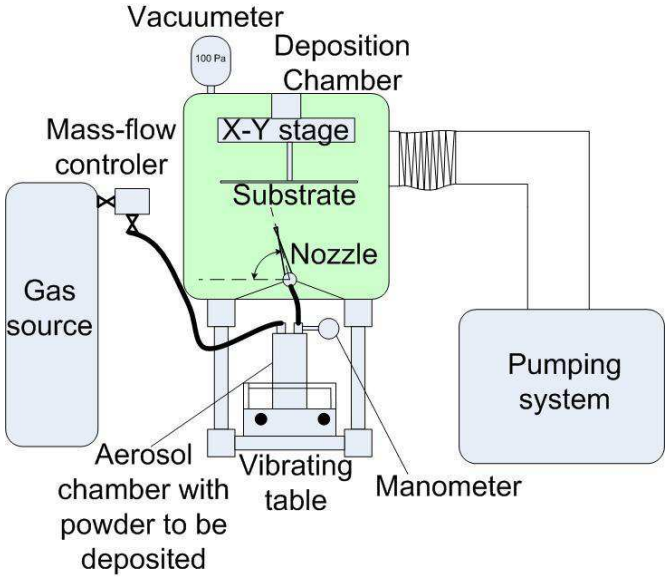

Figure 2. The general schematic of an AD apparatus.

Results and Discussion

SEM images of the surface of the 8YSZ electrolyte and GDC buffer layers after deposition and heat treatment are shown in Figure 3. The deposited films demonstrate a nanocrystalline well-compacted structure without any micro defects. 8YSZ particles were smaller after deposition and the structural units of the resulting films were less than 100 nm. After deposition, most of the GDC particles were small enough that they could not be clearly distinguished with the SEM equipment employed, which means that they were probably smaller than 50 nm. The inhomogeneity of the GDC film surface, which can be seen in Figure 3c, can be explained by an uncrushed particle that deposited on the surface of the film and was then displaced by the following particle stream. If we compare the morphology of the raw deposited films (Figure 3a, c) with the morphology of the prepared powders (Figure 1), we can conclude that the powder particles after impact with the

substrate completely deagglomerate to single crystallites. However, whether there was a reduction in the size of the crystallites themselves cannot be determined for sure. Though tests of the porosity of the deposited films were not conducted, it is believed that their structure after deposition is not gas-tight enough to work as a solid electrolyte membrane for hydrogen-fueled SOFCs. The SEM images of deposited layers after annealing show significant grain growth and a more dense structure. The 8YSZ electrolyte films (Figure 3b) have a grain size of around 1 µm and these films are free of harmful defects, which indicates their good potential as a membrane for SOFCs.

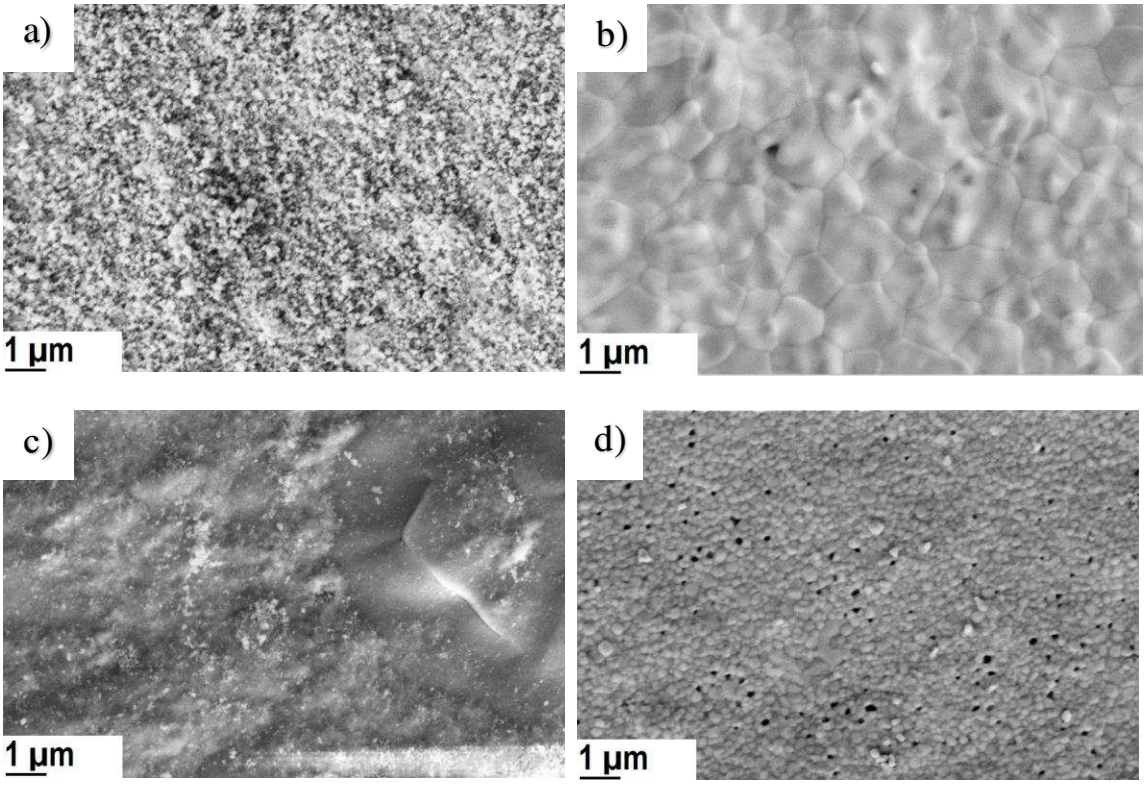

Figure 3. (a) Surface of 8YSZ layer after deposition, (b) surface of 8YSZ layer after deposition and sintering at 1300 °C, (c) surface of GDC layer after deposition, (d) surface of GDC layer after deposition and sintering at 1200 °C.

It is worth mentioning that although it is usually the main objective of AD to deposit gas-tight films without requiring any heat treatment, this is not an absolute necessity for anode-supported SOFCs, as the ceramic support can be heated as needed. Moreover, the nanocrystalline structure of the films deposited by AD is not favorable for charge transfer due to the distributed grain boundaries, so some heat treatment of the films is always desirable. Therefore, it was not the goal of the current research to achieve gas-tight films from the deposition alone, but rather defect-free, thin films with consistent thickness and good adhesion. Sintering temperatures of 1300 °C and 1200 °C for the 8YSZ and GDC layers, respectively, were chosen as temperatures corresponding to the best quality of the bi-layered membrane that will be used as a reference point for future research in the area of sintering temperature reduction. It should be noted that the deposition parameters are strongly dependent on powder morphology, and AD equipment geometry, and can be used without any adjustment only if these factors are similar. Otherwise, parameters from

TABLE I should be regarded only as applicable for AD in general. As mentioned earlier, the reduction of crystallite size was arguable, and the processes that took place during the deposition procedure may not be considered true RTIC because it is widely believed that crystallite size reduction is the inherent characteristic of the RTIC phenomenon (7, 17, 18) and the AD method. However, a reduction in crystallite size may not be necessary in the case of films that are to be sintered at high-temperature, and, in fact, may even be the cause of harmful post-sintering pores and cracks forming as was the case in (19) and was also mentioned in (8). One possible explanation of the post-sintering pores and cracks is the uneven growth of crystallites (20) that underwent the RTIC effect in films deposited using AD due to the presence of anisotropic non-uniform mechanical stresses (21), especially at elevated temperatures (6). In this way, even when the RTIC mechanism is desirable, one should consider that it can cause mechanical stresses in the film and consequent pores and cracks after exposure to elevated temperatures, so a balance must be found. SEM images of cross-sections of the type-1 and type-2 cells after testing are shown in Figure 4. The cross-sections of both types of cells demonstrate thin electrolyte layers with a coarse-grained dense structure and good adhesion to the electrodes. The thicknesses of the layers are about 4 μm for the 8YSZ electrolyte in the type-1 cell, and 2 μm for the 8YSZ electrolyte, and 1 μm for the GDC buffer layer in the type-2 cell. The films have unconnected pores with sizes of less than 100 nm. Note the dense structure of the GDC layer, which is rarely achieved when formed by wet-ceramics techniques (22).

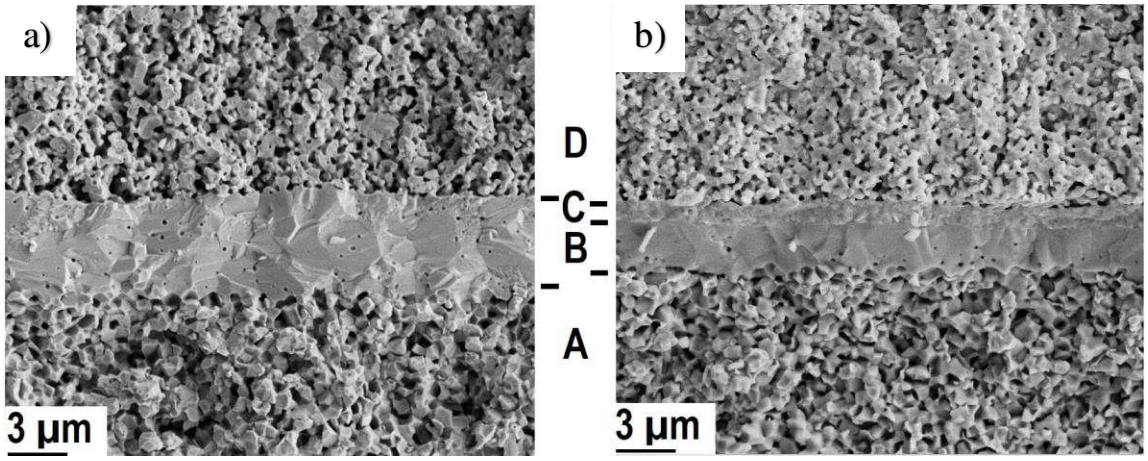

Figure 4. (a) SOFC with 8YSZ electrolyte and LSM cathode (type-1 cell): A – anode functional layer, B – 8YSZ electrolyte, D – LSM cathode; (b) SOFC with 8YSZ electrolyte, GDC buffer layer, and LSC cathode (type-2 cell): A – anode functional layer, B – 8YSZ electrolyte, C – GDC buffer layer, D – LSC cathode.

Measurements of the electrochemical characteristics for both types of cells are shown in Figures 5, and 6. The cells were tested at temperatures of 750 and 800 °C with humidified hydrogen as the fuel and air as the oxidant. The open-circuit voltage was higher than 1 V for both cells at all conditions, which is direct evidence of the uniformly dense structure of the electrolyte and the absence of electron leaks through it. At 800 °C the power density of the type-1 and type-2 cells was higher than 0.40 W/cm^2 and 0.75 W/cm^2, respectively. The large slope of the I-V curve in Figure 5 and the high polarization losses in the impedance spectra (Figure 6) of the type-1 cell is probably a result of low activity, non-ideal structure, and morphology of the composite LSM cathode. The ohmic losses of

the cells can be separated from the total resistance by the high-frequency intercept of the impedance curve with the real axis of the spectrum. The ohmic losses at 750 °C and 800 °C are about 0.175 Ω×cm^2 and 0.150 Ω×cm^2 for the type-1 cell and are about 0.140 Ω×cm^2 and 0.095 Ω×cm^2 for the type-2 cell (Figure 6). In this way, at intermediate temperatures, the contribution of the ohmic resistance is not dominant even for such an active cathode as LSC. The lower ohmic resistance of the type-2 cell can be partially explained by the thinner electrolyte structure and the interaction of the cathode material with the 8YSZ electrolyte at high temperatures in the case of the type-1 cell.

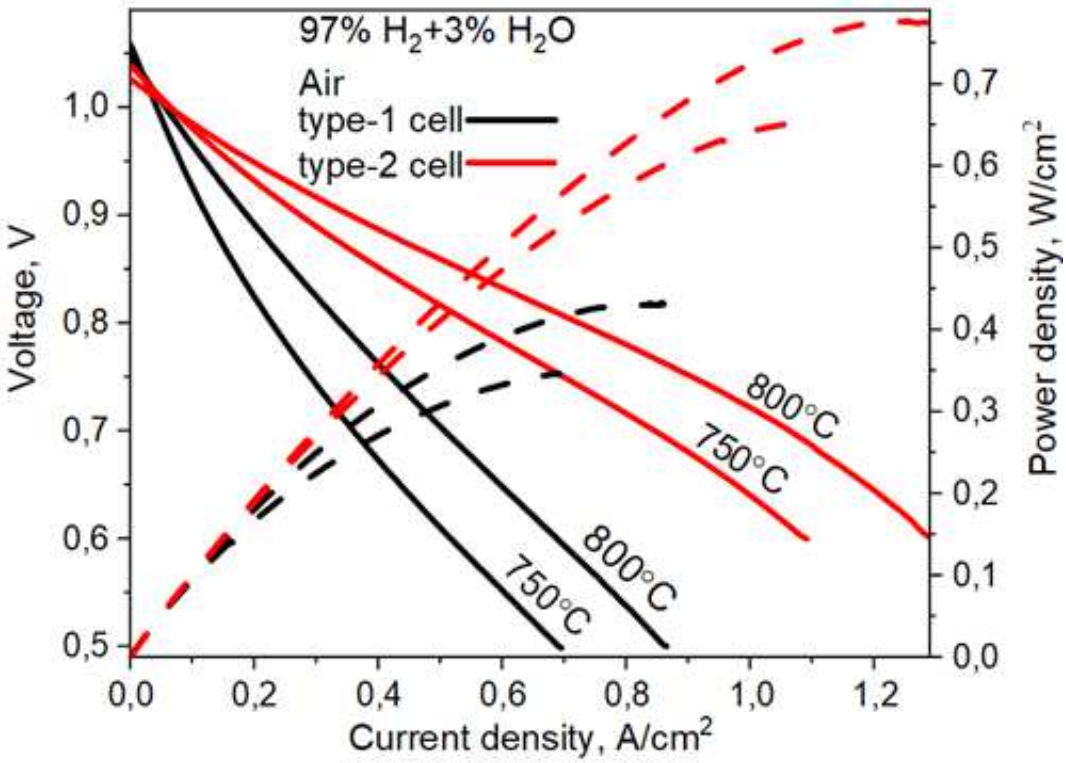

Figure 5. Current-voltage and Power characteristics of the type-1 and type-2 SOFCs.

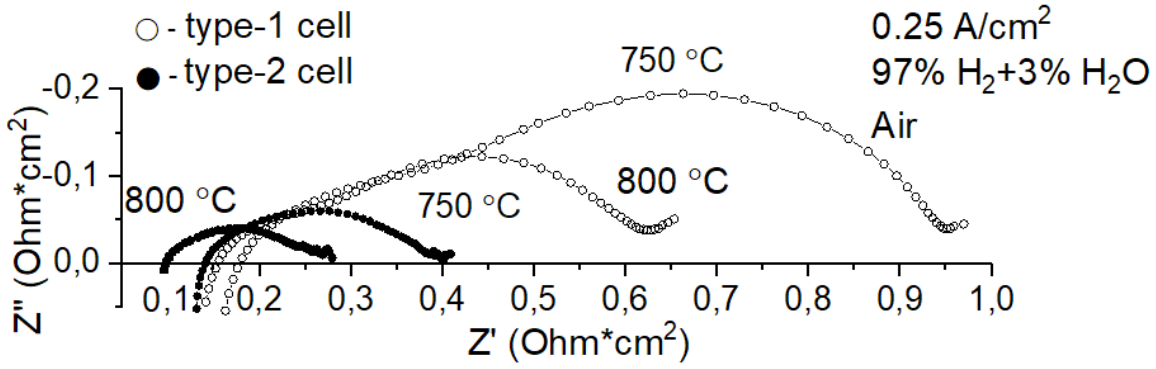

Figure 6. Nyquist plot of the impedance spectra of the type-1 and type-2 SOFCs measured at 750 °C and 800 °C.

Conclusions

The high quality of the electrolytes deposited by AD for both types of SOFCs has been confirmed by SEM, as well as electrochemical measurements, including measurements of current-voltage characteristics and impedance spectroscopy. At a working temperature of 800 °C, anode-supported cells with humidified hydrogen fuel, and air as the oxidant demonstrated an open-circuit voltage of more than 1 V for both types of SOFCs, as well as a specific power density of more than 420 mW/cm^2 and 780 mW/cm^2 for the type-1 and type-2 SOFCs, respectively. The ohmic losses at 750 °C and 800 °C were about 0.175 Ω×cm^2 and 0.150 Ω×cm^2 for the type-1 cell and about 0.140 Ω×cm^2 and 0.095 Ω×cm^2 for the type-2 cell, thus they are not prevailing components of the total resistance even in the case of such an active cathode as LSC.

The results suggest that the AD method has potential to be an inexpensive, easily scalable industrial technique for thin-film electrolyte deposition for intermediate temperature SOFCs. The RTIC phenomenon in the form of a decrease in the crystallite size is not a necessary condition in the case of films that will go through high-temperature heat treatment. Moreover, a reduction in the size of the crystallites may even cause post-sintering pore and crack formation. Future research will include scaling-up the electrolyte deposition to substrates with an area of 100x100 mm^2, research in the area of reducing the sintering temperatures of electrolytes to 900 °C while preserving their hermeticity and conductive properties, and a techno-economic analysis of how the use of AD impacts cell fabrication costs.

Acknowledgments

This work was supported by the Russian Scientific Foundation grant 17-79-30071 “Scientifically grounded optimization of power and mass-dimensional characteristics of planar SOFC stacks and development of fuel processor for highly-efficient transport and stationary power plants”.

References

1. S. Kang., J. Lee, G. Y. Cho, Y. Kim, S. Lee, S. W. Cha, and J Bae, *Int. J. Hydrog. Energy*, **45**, 33980 (2020).
2. D. Y. Jang, M. Kim, J. W. Kim, K. Bae, J. W. Son, M. V. Schlupp, and J. H. Shim, *J. Electrochem. Soc.*, **164**, F484 (2017).
3. D. Das, B. Bagchi, and R. N. Basu, *J. Alloys Compd.*, **693**, 1220 (2017).
4. R. Hui, Z. Wang, O. Kesler, L. Rose, J. Jankovic, S. Yick, R. Maric, and D. Ghosh, *J. Power Sources*, **170**, 308 (2007).
5. P. Coddet, H.-L. Liao, and C. Coddet, *Adv. Manuf.*, **2**, 212 (2014).
6. J. Akedo and M. Lebedev, *Jpn. J. Appl. Phys.*, **38**, 5397 (1999).
7. J. Akedo, *J. Am. Ceram. Soc.*, **89**, 1834 (2006).
8. J. Exner, T. Nazarenus, D. Hanft, J. Kita, and R. Moos, *Adv. Mater.*, **32**, 1908104 (2020).
9. J. Exner, J. Kita, and R. Moos, *J. Mater. Sci.*, **54**, 13619 (2019).

10. I. S. Erilin, D. A. Agarkov, I. N. Burmistrov, V. E. Pukha, D. V. Yalovenko, N. V. Lyskov, and S. I. Bredikhin, *Mater. Lett.*, **266**, 127439 (2020).
11. M. A. Sukeshini, R. Cummins, T. L. Reitz, and R. M. Miller, *J. Am. Ceram. Soc.*, **92**, 2913 (2009).
12. S. Onbilgin, B. Timurkutluk, C. Timurkutluk, and S. Celik, *Int. J. Hydrog. Energy*, **45**, 35162 (2020).
13. A. A. Solovyev, A. M. Lebedynskiy, A. V. Shipilova, I. V. Ionov, E. A. Smolyanskiy, A. L. Lauk, and G. E. Remnev, *Int. J. Hydrog. Energy*, **44**, 30636 (2019).
14. X.-V. Nguyen, C. T. Chang, G. B. Jung, S. H. Chan, W. C. W. Huang, K. J. Hsiao, and I. Kao, *Energies*, **9**, 701 (2016).
15. S. I. Bredikhin, D. A. Agarkov, E. Agarkova, I. Burmistrov, A. Cherkasov, V. Pukha, and N. Lyskov, *ECS Trans.*, **91(1)**, 403 (2019).
16. J. Akedo, *J. Ceram. Soc. JAPAN*, **128**, 101 (2020).
17. J. Exner, M. Schubert, D. Hanft, J. Kita, and R. Moos, *J. Eur. Ceram. Soc.,* **39**, 592 (2019).
18. J. Akedo, *Mater. Sci. Forum,* **449**, 43 (2004).
19. J.-J. Choi, J. H. Choi, J. Ryu, B. D. Hahn, J. W. Kim, C. W. Ahn, and D. S. Park, *J. Eur. Ceram. Soc.*, **32**, 3249 (2012).
20. M. F. Yan, R. M. Cannon Jr, H. K. Bowen, and U. Chowdhry, Mater. Sci. Eng., ***60***, 275 (1983).
21. F. Uyar, S. Wilson, M. Winning, and A. D. Rollett, *Mater. Sci. Forum*, **715**, 197 (2012).
22. Y. Leng, S. Chan, S. Jiang, and K. Khor, *Solid State Ion.*, **170**, 9 (2004).